Piqueras, MA.; Company Rossi, R.; Jódar Sánchez, LA. (2020). Solving two-phase freezing Stefan problems: Stability and monotonicity. Mathematical Methods in the Applied Sciences. 43(14):7948-7960. https://doi.org/10.1002/mma.5787

Received ; | Revised ; | Accepted

DOI: xxx/xxxx

ARTICLE TYPE

Solving two-phase freezing Stefan problems: stability and monotonicity

M.-A. Piqueras | R. Company* | L. Jódar

[1]Instituto de Matemática Multidisciplinar, Universitat Politècnica de València, Camino de Vera s/n, 46022 Valencia, Spain

Correspondence
*R. Company. Email: rcompany@imm.upv.es

Summary

The two-phase Stefan problems with phase formation and depletion are special cases of moving boundary problems with interest in science and industry. In this work, we study a solidification problem, introducing a front-fixing transformation. The resulting nonlinear partial differential system involves singularities, both at the beginning of the freezing process and when the depletion is complete, that are treated with special attention in the numerical modelling. The problem is decomposed in three stages, in which implicit and explicit finite difference schemes are used. Numerical analysis reveals qualitative properties of the numerical solution spatial monotonicity of both solid and liquid temperatures and the evolution of the solidification front. Numerical experiments illustrate the behaviour of the temperatures profiles with time, as well as the dynamics of the solidification front.

KEYWORDS:
Two-phase Stefan problem, Nonlinear partial differential system, Numerical modelling, Finite difference, Numerical analysis.

1 | INTRODUCTION

Free boundary problems are used to model a wide scenario of applications coming from biophysics, chemistry, astronomy, materials science and ecology [1]. These problems are characterized by the fact that the moving boundary is an unknown part of the problem, [2]. A subset of these kind of models are the so-called Stefan problems describing several phenomena in nature, science and society, such as the dentritic solidification problem [3], cryosurgical treatment of tumors in medicine [4], American option pricing problem [5], desalination of sea water [6] and heat transfer problems with phase changes related to melting and freezing problems [7]. Exact analytical solution of these problems is only available in some particular cases stated in a semi-infinite domain, for instance the well known Lamé-Clapeyron-Stefan problem, see [1], chapter 3. Analytic solutions for two-phase Stefan problems using similarity solutions have been proposed in [8], including source terms in the problem formulation. Apart from the analytical methods, a wide class of semianalytical methods have been proposed to solve more general problems, [9,10,11,12], method of perturbation, [13,14].

Concerning the treatment of the moving boundary there are two main types of methods, [15]. The front-tracking method is based on the continuous updating of the moving boundary, see chapter 4 of [1]; inside this method, it is important to mention the variable space grid method [16], the variable time step method [17] and the heat balance integral method [18]. Another approach is to use a fixed domain formulation or front-fixing based on a transformation of the original problem, for instance the boundary immobilization method, [19], chapter 5 of [1], isotherm migration method, [20,21], and enthalpy method, [9,22,23]. Both approaches the front-tracking and the front-fixing have been performed using finite difference or finite elements schemes.

The application of the front-fixing technique to a two-phase problem presents two challenges due to the appearance of singularities in the transformed partial differential equations (PDEs): Firstly, the correct initialization when the first phase initially has zero thickness, and on the other hand, the treatment of the depletion of the second phase close to the extinction time. The authors in [15], consider the one-phase problem by using front-fixing approaches together with explicit finite difference schemes, overcome the initialization difficulty taking the analytic solution of the semi-infinite problem in this starting stage for the temperature as well as for the evolution of the moving boundary from the starting zero thickness. The correct initialization and depletion of the two-phase Stefan problem has been recently addressed by [24] by using the Keller box implicit difference scheme, see [25].

The numerical modelling proposed in this paper does not need the analytic solution of the underlying semi-infinite problem but only the hypothesis of the $\sqrt{t}$-law behaviour of the moving boundary in the initialization of the problem. The treatment of the depletion is also addressed through a split of the process in three stages: the first one related to the initialization, the second one embracing almost the entire process of solidification and the third stage dealing with the depletion of the liquid phase until extinction. As the best model can be wasted with a disregarded analysis, it motivates to pay attention to the numerical analysis. In this address we study qualitative properties of the numerical solution and stability. In fact, we construct an implicit difference scheme in the first stage and we give a stability condition in terms of the stepsizes of the discretized variables. Furthermore, the scheme mirrors the property that the temperature in the solid phase is greater than the one in the left end and smaller than the phase-change temperature. In addition, in the liquid phase, the temperatures described by the numerical solution lies between the phase-change temperature and the initial temperature of the liquid. Otherwise, in the next stages we use an explicit conditionally stable difference scheme and monotonicity properties are studied, i.e., as the material is cooling at the left end, the temperature grows with the space at every temporal level. It is important to point out that this advantage of getting information about qualitative properties arises from the explicit difference scheme versus other approaches such as implicit schemes, finite-element, meshless methods, etc.

Apart from the numerical analysis, this numerical modelling approach has the potential application of dealing with more complicated problems where the analytic solution of the corresponding semi-infinite problem is not available.

Consider the two-phase model describing the freezing of a liquid in one spatial dimension occupying initially the region $0 \leq x \leq a$. At the initial time, the temperature of the material is uniform, T_h, higher than the phase-change temperature, written as T_f. The material is cooled at the point $x = 0$ by imposing a constant temperature T_c, lower than the phase-change temperature, T_f.

The continuous model with phase formation and depletion is formulated as,

$$\rho c_s \frac{\partial T_s}{\partial t} = \kappa_s \frac{\partial^2 T_s}{\partial x^2}, \quad 0 < x < S(t), \quad t > 0, \tag{1}$$

$$\rho c_l \frac{\partial T_l}{\partial t} = \kappa_l \frac{\partial^2 T_l}{\partial x^2}, \quad S(t) < x < a, \quad t > 0. \tag{2}$$

The boundary conditions are expressed as

$$T_s(0,t) = T_c, \quad t > 0, \tag{3}$$

$$T_s(S(t),t) = T_l(S(t),t) = T_f, \quad t > 0, \tag{4}$$

and

$$\frac{\partial T_l}{\partial x}(a,t) = 0, \quad t > 0. \tag{5}$$

Note that Dirichlet boundary condition (3) means an isothermal cooling at the left end of the domain while the homogeneous Neumann boundary condition (5) expresses that the right end of the domain is perfectly insulated so there is not heat flow. The initial conditions are given by

$$T_l(x,0) = T_h, \quad 0 \leq x \leq a, \quad S(0) = 0. \tag{6}$$

Finally, the so-called Stefan condition, expressing the heat balance on the interface, takes the form

$$\rho C_m \frac{dS}{dt} = \kappa_s \frac{\partial T_s}{\partial x} - \kappa_l \frac{\partial T_l}{\partial x}, \quad x = S(t), \quad t > 0. \tag{7}$$

Here, T_s denotes the solid phase temperature, κ_s is the thermal conductivity of the solid, c_s is the specific heat capacity of the solid phase. Analogously, using the same notation for the liquid phase, T_l denotes the liquid phase temperature, κ_l the thermal conductivity of the liquid and c_l the specific heat capacity of the liquid phase. Regarding the mass density of the material, it is assumed to have the same value ρ, both in solid and liquid state. The value C_m represents the latent heat of fusion. $S(t)$ indicates the location of the solidification front.

Comparing the scenario of the freezing problem (1)-(7), where we have an isothermal cooling at the left solid end (3), together with an insulated right liquid end (5), then the solidification front $S(t)$ is an increasing function and thus,

$$\rho C_m \frac{dS}{dt} > 0, \quad t > 0. \tag{8}$$

To transform our problem into a dimensionless one, the following nondimensional variables in space and time are used:

$$y = \frac{x}{a}, \quad \tilde{t} = \frac{\kappa_l t}{\rho c_l a^2}, \quad \tilde{S}(\tilde{t}) = \frac{S(t)}{a}. \tag{9}$$

Consider an arbitrarily small value S_0, $0 < S_0 < a$, a relative quantity $R_0 = S_0/a$ and let us introduce the new temporal variable and the transformed solidification front, respectively

$$\tau = \tilde{t}/R_0^2, \quad \sigma(\tau) = R(\tau)/R_0, \quad R(\tau) = \tilde{S}(\tilde{t}). \tag{10}$$

Also, the unknowns for the temperatures in the solid and liquid phases, respectively, are expressed as

$$\hat{U}_s = \frac{T_s - T_f}{T_f - T_c}, \quad \hat{U}_l = \frac{T_l - T_f}{T_h - T_f}. \tag{11}$$

After these changes, and simplifying the notation by using the parameters

$$\kappa = \frac{\kappa_l c_s}{\kappa_s c_l}, \quad K = \frac{\kappa_s (T_f - T_c)}{\kappa_l (T_h - T_f)}, \quad \beta = \frac{C_m}{c_l (T_h - T_f)}, \tag{12}$$

the problem (1)-(7) becomes

$$\frac{\partial \hat{U}_s}{\partial \tau} = \frac{R_0^2}{\kappa} \frac{\partial^2 \hat{U}_s}{\partial y^2}, \quad 0 < y < R_0 \sigma(\tau), \quad \tau > 0, \tag{13}$$

$$\frac{\partial \hat{U}_l}{\partial \tau} = R_0^2 \frac{\partial^2 \hat{U}_l}{\partial y^2}, \quad R_0 \sigma(\tau) < y < 1, \quad \tau > 0, \tag{14}$$

subject to the boundary conditions

$$\hat{U}_s(0, \tau) = -1, \quad \tau > 0, \tag{15}$$

$$\hat{U}_s(R_0 \sigma(\tau), \tau) = \hat{U}_l(R_0 \sigma(\tau), \tau) = 0, \quad \tau > 0, \tag{16}$$

and

$$\frac{\partial \hat{U}_l}{\partial y}(1, \tau) = 0, \quad \tau > 0, \tag{17}$$

and the new initial conditions

$$\hat{U}_l(y, 0) = 1, \quad 0 \le y \le 1, \quad \sigma(0) = 0. \tag{18}$$

Finally, the Stefan condition is written as

$$\frac{d\sigma}{d\tau} = \frac{K R_0}{\beta} \frac{\partial \hat{U}_s}{\partial y} - \frac{R_0}{\beta} \frac{\partial \hat{U}_l}{\partial y}, \quad y = R_0 \sigma(\tau), \quad \tau > 0. \tag{19}$$

The main Section 2 begins with the front-fixing transformation of the moving boundary problem. Then, the numerical modelling is developed by splitting the solidification process in three stages: initialization, progress stage and depletion. In both stages, discretization, numerical analysis, including the study of qualitative properties of the numerical solution, the stability and simulation are performed. Illustrative numerical experiments are also included. The paper ends with a conclusion section.

2 | FRONT-FIXING TRANSFORMATION AND NUMERICAL MODELLING

The correct initialization of the solidification front requires that $S(0) = 0$, i.e. $\sigma(0) = 0$, where

$$\sigma(\tau) = R(\tau)/R_0. \tag{20}$$

Let us consider the front-fixing transformation ([1,19])

$$z(y,\tau)=\begin{cases}\dfrac{y-\sigma(\tau)R_0}{\sigma(\tau)R_0}, & 0\le y\le\sigma(\tau)R_0,\quad \tau\ge 0,\\[2ex] \dfrac{y-\sigma(\tau)R_0}{1-\sigma(\tau)R_0}, & \sigma(\tau)R_0\le y\le 1,\quad \tau\ge 0.\end{cases}\tag{21}$$

As a result of trasform (21), the moving boundary problem (13)-(19) turns into another one that is posed in a fixed immobilized domain, $-1\le z\le 1$, $\tau\ge 0$, that causes difficulties in the initialization and in the depletion. Indeed, the transformation (21) involves singularities when $\tau=0$, $\sigma(0)=0$, and when $\sigma(\tau)=R_0^{-1}$. The difficulty about $t=0$ can be overcome without considering the analytic solution of the corresponding semi-infinite two-phase Lamé-Clapeyron-Stefan problem, [1,26], but only assuming that the solidification front in the nondimensional problem follows the behaviour $C\sqrt{\tau}$ in a small neighbourhood close to $\tau=0$, where C is obtained throughout numerical modelling specified later. Another important issue is the numerical treatment of the problem close to the extinction time τ_e, [26], without using the solution of the semi-infinite problem. In fact, in agreement with the comment by the authors of [24], p. 270, we neglect the liquid phase starting from a time $\tau_1<\tau_e$. The selection of this critical time τ_1 is performed in order to guarantee the numerical stability of the solution.

Thus, the numerical modelling of the problem is developed in three stages. The first stage corresponds to the correct initialization of the solidification process, that is performed using an implicit scheme for both purposes, the estimation of C as well as obtaining the temperature of the solid and the liquid phases until a time τ_0 such that the solidification front has reached the relative value R_0.

Then, the second stage corresponds to the evolution of the two-phase problem until we reach time τ_1. Note that in this second stage we need to compute both the temperature of solid and liquid phases, as well as the solidification front. This computation is performed using an explicit method that, apart from being quick and no requiring initialization guess, as it occurs with the implicit methods, it will be particularly convenient to study numerical properties of the numerical solution.

Finally, in the last stage we neglect the liquid phase and we study the behaviour of the solidification front and the temperature of the solid region until the extinction time, continuing with the explicit scheme.

Let us choose an arbitrarily small value $S_0>0$ and denote $t_0>0$ the time such that $S(t_0)=S_0$, following the $\sqrt{t}$-law, see equation (3.10) of page 102 of [1] and equation (12) of page 188 of [26]. Taking τ_0 the corresponding transformed time throughout (10) one gets,

$$\sigma(\tau_0)=\sigma_0=\frac{R(\tau_0)}{R_0}=\frac{a\tilde{S}(\tilde{t}_0)}{S_0}=1.\tag{22}$$

Therefore, we assume that the solidification front follows a behaviour $\sigma(\tau)=C\sqrt{\tau}$ in a short first stage $0\le\tau\le\tau_0$, dependent on the initial prefixed value S_0. From (9)-(20), one gets

$$\sigma(\tau)=C\sqrt{\tau},\quad 0\le\tau\le\tau_0=\frac{\tilde{t}_0}{R_0^2}=\frac{1}{C^2},\tag{23}$$

and the value C is obtained numerically as it will be explained later. Note that, during this stage, $0\le\sigma(\tau)\le 1$. Hereinafter the tilde in $\tilde{t}$ is dropped.

Hence, from the above variable change (20), transformation (21) and the relationships

$$\hat{U}_s(y,\tau)=U_s(z,\tau),\quad \hat{U}_l(y,\tau)=U_l(z,\tau),\tag{24}$$

problem (13)-(19) takes the form

$$\frac{\partial U_s}{\partial\tau}=\frac{\sigma'(\tau)(1+z)}{\sigma(\tau)}\frac{\partial U_s}{\partial z}+\frac{1}{\kappa\sigma^2(\tau)}\frac{\partial^2U_s}{\partial z^2},\quad -1<z<0,\quad \tau>0,\tag{25}$$

$$\frac{\partial U_l}{\partial\tau}=\frac{\sigma'(\tau)R_0(1-z)}{1-\sigma(\tau)R_0}\frac{\partial U_l}{\partial z}+\frac{R_0^2}{(1-\sigma(\tau)R_0)^2}\frac{\partial^2U_l}{\partial z^2},\quad 0<z<1,\quad \tau>0,\tag{26}$$

satisfying the boundary conditions

$$U_s(-1,\tau)=-1,\quad \tau>0,\tag{27}$$

$$U_s(0,\tau)=U_l(0,\tau)=0,\quad \tau>0,\tag{28}$$

and

$$\frac{\partial U_l}{\partial z}(1,\tau)=0,\quad \tau>0, \tag{29}$$

together with the initial conditions

$$U_s(z,0)=-1,\quad -1\le z\le 0,\quad U_l(z,0)=1,\quad 0\le z\le 1,\quad \sigma(0)=0, \tag{30}$$

and the Stefan condition at the solidification front

$$\frac{d\sigma}{d\tau}=\frac{K}{\beta\sigma(\tau)}\frac{\partial U_s}{\partial z}-\frac{R_0}{\beta(1-\sigma(\tau)R_0)}\frac{\partial U_l}{\partial z},\quad z=0,\quad \tau>0. \tag{31}$$

2.1 | First stage numerical modelling

In the first stage, $0\le\tau\le\tau_0$, using the $\sqrt{\tau}$-law (23) for the dynamics of the solidification front, problem (25)-(31) becomes

$$\frac{\partial U_s}{\partial\tau}=\frac{1+z}{2\tau}\frac{\partial U_s}{\partial z}+\frac{1}{\kappa C^2\tau}\frac{\partial^2 U_s}{\partial z^2},\quad -1<z<0,\quad 0<\tau<\tau_0, \tag{32}$$

$$\frac{\partial U_l}{\partial\tau}=\frac{CR_0(1-z)}{2\sqrt{\tau}(1-CR_0\sqrt{\tau})}\frac{\partial U_l}{\partial z}+\frac{R_0^2}{(1-CR_0\sqrt{\tau})^2}\frac{\partial^2 U_l}{\partial z^2},\quad 0<z<1,\quad 0<\tau<\tau_0, \tag{33}$$

together with boundary and initial conditions (27)-(29) and (30), respectively, and the Stefan condition with $\sqrt{\tau}$-law

$$\frac{C}{2\sqrt{\tau}}=\frac{K}{\beta C\sqrt{\tau}}\frac{\partial U_s}{\partial z}+\frac{R_0}{\beta(1-CR_0\sqrt{\tau})}\frac{\partial U_l}{\partial z},\quad z=0,\quad 0<\tau<\tau_0, \tag{34}$$

that is going to be used to estimate numerically the value of C.

In order to circumvent the singularity of equations (32)-(33) at $\tau=0$, we use a fully implicit scheme, backward in time and centred in space. The numerical domain is partitioned by the grid

$$\Omega=\{(z_j,\tau^n),\quad -M\le j\le M,\quad 0\le n\le n_0\}, \tag{35}$$

with $h=\Delta z=1/M$; $\Delta\tau=\tau_0/n_0$, and $z_j=jh$, $\tau^n=n\Delta\tau$, where M and n_0 are positive integers. Numerical approximations of the unknowns are denoted by: $u^n_{s,j}\approx U_s(z_j,\tau^n)$, $u^n_{l,j}\approx U_l(z_j,\tau^n)$, $\sigma^n\approx\sigma(\tau^n)$.

To preserve the second order accuracy at the solidification front $z=0$, we take left and right side approximations with three points, for the solid and liquid phase, respectively:

$$\frac{3u^n_{s,0}-4u^n_{s,-1}+u^n_{s,-2}}{2h}\approx\frac{\partial U_s}{\partial z}(0,\tau^n),\quad \frac{-3u^n_{l,0}+4u^n_{l,1}-u^n_{l,2}}{2h}\approx\frac{\partial U_l}{\partial z}(0,\tau^n). \tag{36}$$

Boundary conditions (27)-(29) are discretized as

$$u^n_{s,-M}=-1,\quad u^n_{s,0}=u^n_{l,0}=0,\quad \frac{u^n_{l,M-1}-u^n_{l,M+1}}{2h}=0,\quad 0\le n\le n_0, \tag{37}$$

where $z_{M+1}=(M+1)h$ is an artificial mesh point and the value $u^n_{l,M+1}$ is eliminated under the standard assumption that the equation (33) is also satisfied at the boundary $z_M=1$,[27] .

From the above comments, one gets a tridiagonal algebraic system

$$\begin{cases} A^{n+1}U_s^{n+1}=U_s^n,\\ \qquad\qquad 0\le n\le n_0-1,\\ B^{n+1}U_l^{n+1}=U_l^n, \end{cases} \tag{38}$$

where $U_s^n=[u^n_{s,-M},u^n_{s,-M+1},\dots,u^n_{s,0}]^T$, $U_l^n=[u^n_{l,0},u^n_{l,1},\dots,u^n_{l,M}]^T$, and

$$A^n=A^n(C)=\left(A^n_{i,j}\right)_{-M\le i,j\le 0},\quad B^n=B^n(C)=\left(B^n_{i,j}\right)_{0\le i,j\le M}, \tag{39}$$

are tridiagonal matrices of size $(M+1)\times(M+1)$, whose nonzero entries are

$$\begin{aligned} &A^n_{-M,-M}=A^n_{0,0}=1,\\ &A^n_{j,j-1}=-(a^n-c^n_j);\quad A^n_{j,j}=1+2a^n;\quad A^n_{j,j+1}=-(a^n+c^n_j),\\ &-M+1\le j\le -1, \end{aligned} \tag{40}$$

$$
\begin{aligned}
&B^n_{0,0} = 1; \quad B_{M,M-1} = -2b^n, \quad B_{M,M} = 1 + 2b^n, \\
&B^n_{j,j-1} = -(b^n - d^n_j); \quad B^n_{j,j} = 1 + 2b^n; \quad B^n_{j,j+1} = -(b^n + d^n_j), \\
&1 \le j \le M - 1.
\end{aligned} \tag{41}
$$

Coefficients appearing in (40)-(41), depending on the step sizes h and $\Delta\tau$, have the form:

$$
\begin{aligned}
&a^n = \frac{1}{\kappa C^2 n h^2}, \quad c^n_j = \frac{z_j + 1}{4nh}, \\
&b^n = \frac{R_0^2 \Delta\tau}{h^2(1 - CR_0\sqrt{n\Delta\tau})^2}, \quad d^n_j = \frac{CR_0\sqrt{\Delta\tau}(1 - z_j)}{4\sqrt{n}h(1 - CR_0\sqrt{n\Delta\tau})}.
\end{aligned} \tag{42}
$$

A^{n+1} and B^{n+1} of (38) have all the row sums positive from (40)-(41). Note that if

$$
\mathrm{C1}: a^{n+1} - c^{n+1}_j \ge 0, \quad \mathrm{C2}: b^{n+1} - d^{n+1}_j \ge 0, \quad 0 \le n \le n_0 - 1, \tag{43}
$$

respectively, matrices A^{n+1} and B^{n+1} are Z-matrices, i.e., they have all entries nonpositive out of the main diagonal. Then, under conditions C1 and C2, matrices A^{n+1} and B^{n+1} are nonsingular M-matrices and their inverses $(A^{n+1})^{-1}$ and $(B^{n+1})^{-1}$ are nonnegative,[28] and[29], chap. 6. This property guarantees that the sign of the vector solution of system (38) is preserved.

From (42) it is easy to check that conditions (43) are verified for all j and n if step sizes satisfy the condition

$$
h \le \min\{h_1, h_2\}, \quad h_1 = \frac{4}{\kappa C^2}, \quad h_2 = \frac{4R_0\sqrt{\Delta\tau}}{C}. \tag{44}
$$

Apart from the sign stability, the implicit scheme (38) guarantees the $\|\cdot\|_\infty$-stability of the solution, in the sense that $\|U^n_s\|_\infty$ and $\|U^n_l\|_\infty$ remain bounded for all n. In fact, matrices A^{n+1} and B^{n+1} have the property that all their row sums are equal to one. It is easy to check that then, their positive inverses also satisfy the same property and $\|(A^n)^{-1}\|_\infty = \|(B^n)^{-1}\|_\infty = 1$. In fact,

$$
\|U^{n+1}_s\|_\infty = \|(A^{n+1})^{-1}U^n_s\|_\infty \le \|(A^{n+1})^{-1}\|_\infty \|U^n_s\|_\infty. \tag{45}
$$

Then,

$$
\|U^n_s\|_\infty \le \|U^0_s\|_\infty = 1, \quad 0 \le n \le n_0, \tag{46}
$$

and analogously,

$$
\|U^n_l\|_\infty \le \|U^0_l\|_\infty = 1, \quad 0 \le n \le n_0. \tag{47}
$$

Furthermore, from (46)-(47) and taking into account that $U^n_s \le 0$, $U^n_l \ge 0$, one gets

$$
-1 \le u^n_{s,j} \le 0, \quad -M \le j \le 0; \quad 0 \le u^n_{l,j} \le 1, \quad 0 \le j \le M, \tag{48}
$$

for all time steps $0 \le n \le n_0$.

This means that the numerical solution preserves the property that the temperature in the solid phase is greater than the boundary value, and for the liquid phase, the temperature is below the initial temperature at the right boundary.

In order to estimate the value of the constant C related to the $\sqrt{\tau}$-law, i.e $\sigma(\tau) = C\sqrt{\tau}$, we take the first time step of the system (38) together with the linking discretization of Stefan condition (34), building a system of $2M+3$ nonlinear algebraic equations,

$$
\begin{cases}
A^1 U^1_s = U^0_s, \\
B^1 U^1_l = U^0_l, \\
\dfrac{C}{2} = \dfrac{K}{\beta C}\Delta u^1_{s,0} + \dfrac{R_0\sqrt{\Delta\tau}}{\beta(1 - CR_0\sqrt{\Delta\tau})}\Delta u^1_{l,0},
\end{cases} \tag{49}
$$

where

$$
\Delta u^1_{s,0} = \frac{3u^1_{s,0} - 4u^1_{s,-1} + u^1_{s,-2}}{2h}, \quad \Delta u^1_{l,0} = \frac{-3u^1_{l,0} + 4u^1_{l,1} - u^1_{l,2}}{2h}, \tag{50}
$$

on the $2M + 3$ unknowns

$$
\left\{\{u^1_{s,j}, -M \le j \le 0\}, \{u^1_{l,j}, 0 \le j \le M\}, C\right\}. \tag{51}
$$

Solving the system (49)-(50) with the MATLAB optimization algorithm Fsolve, one gets the temperature at the mesh points in the first time level $n = 1$ as well as the value of C. It is clear that the value of C depends on the parameters h, $\Delta\tau$ for a fixed chosen solidified fraction R_0 of the material at the end of the first stage. In the Table 1, we show that for different choices of the

h	0.0050	0.0040	0.0030	0.0020	0.0010
$\Delta\tau$	0.0480	0.0325	0.0200	0.0100	0.0026
C	0.7762	0.7728	0.7684	0.7616	0.7596

TABLE 1 Dependence of C on the step sizes when the parameters of the model are $\kappa = K = \beta = 1$.

step sizes discretizations verifying the stability condition (43), one gets values of the constant C close to the theoretical value of the semi-infinite two-phase Lamé-Clapeyron-Stefan problem, see [1], equation (3.11), p. 102.

Next example illustrates the temperature profile in both phases solid and liquid, obtained by the numerical scheme (38) at the end of the fist stage.

Example 1 Numerical solution of system (38) for the last time step n_0 of this first stage such that $\tau_0 = n_0\Delta\tau$, is shown in Figure 1 . The parameters are $\kappa = K = \beta = 1$; $\Delta\tau = 0.01$, $h = 0.002$, $R_0 = 0.03$ and the value C, previously obtained, is $C = 0.7616$. Note that $R_0 = 0.03$ means that 3% of the material has solidified. From (23), $\tau_0 = 1.72404$.

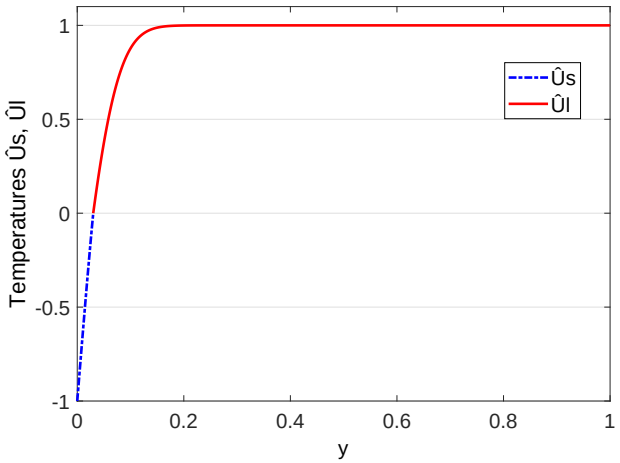

FIGURE 1 Numerical solutions for example 1 at the end of the first stage.

2.2 | Second stage numerical modelling

Once the initialization difficulties have been overcome, we address the second stage, where an explicit scheme is used for the numerical solution of equations (25)-(26) with the Stefan condition (31). For this stage, let us take a time step k and the discretized temporal variable $\tau^n = \tau_0 + (n - n_0)k$, $n_0 \le n \le n_1$, where n_1 is the final time level to be determined by the stability requirements. Note that here, the discretized initial conditions coincide with the final ones of the first stage, while the boundary conditions remain unaltered, (37). For the spatial step h and the time step k, the explicit scheme for the interior points takes the form

$$u_{m,j}^{n+1} = a_{m,j}^n u_{m,j-1}^n + b_{m,j}^n u_{m,j}^n + c_{m,j}^n u_{m,j+1}^n, \quad m = s, l, \quad n_0 \le n \le n_1 - 1, \tag{52}$$

where

$$\begin{aligned}
&a^n_{s,j} = \alpha^n - (1+z_j)\beta^n, \quad b^n_{s,j} = 1 - 2\alpha^n, \quad c^n_{s,j} = \alpha^n + (1+z_j)\beta^n,\\
&\alpha^n = \frac{k}{h^2\kappa(\sigma^n)^2}, \quad \beta^n = \frac{\sigma^{n+1}-\sigma^n}{2h\sigma^n};\\
&a^n_{l,j} = \gamma^n - (1-z_j)\delta^n, \quad b^n_{l,j} = 1 - 2\gamma^n; \quad c^n_{l,j} = \gamma^n + (1-z_j)\delta^n,\\
&\gamma^n = \frac{k}{h^2(\rho_0-\sigma^n)^2}, \quad \delta^n = \frac{\sigma^{n+1}-\sigma^n}{2h(\rho_0-\sigma^n)};
\end{aligned} \tag{53}$$

and

$$\rho_0 = \frac{1}{R_0}. \tag{54}$$

In the above notation, $m = s$ or $m = l$, where s holds for the material in the solid phase and l for the liquid phase. Note that for the solid phase $-M+1 \le j \le -1$, while for the liquid phase $1 \le j \le M$, involving the value $u^n_{l,M+1}$ at the fictitious mesh point z_{M+1}. Finally, the discretization of the Stefan-like condition (31) for obtaining the evolution of the solidification front takes the form

$$\frac{\sigma^{n+1}-\sigma^n}{k} = \frac{K}{\beta\sigma^n}\Delta u^n_{s,0} - \frac{1}{\beta(\rho_0-\sigma^n)}\Delta u^n_{l,0}, \quad n_0 \le n \le n_1 - 1, \tag{55}$$

where

$$\Delta u^n_{s,0} = \frac{3u^n_{s,0} - 4u^n_{s,-1} + u^n_{s,-2}}{2h}, \quad \Delta u^n_{l,0} = \frac{-3u^n_{l,0} + 4u^n_{l,1} - u^n_{l,2}}{2h}, \tag{56}$$

are the second order approximations of the involved one-sided partial derivatives in (31).

Now we study sufficient conditions for the positivity of coefficients in (52), because this fact guarantees the preservation of the sign of the solutions (negative for the solid phase and positive for the liquid one). From (52)-(53), the increasing behaviour of the solidification front and (22), the coefficient $b^n_{s,j}$ becomes positive if

$$k < \frac{\kappa h^2}{2}. \tag{57}$$

Using (53), Stefan condition (55) and the fact that both expressions $h\Delta u^n_{l,0}$ and $h\Delta u^n_{l,0}$ are $\mathcal{O}(h)$, it holds

$$\frac{\beta^n}{\alpha^n} = \frac{\kappa h\sigma^n(\sigma^{n+1}-\sigma^n)}{2k} = \frac{\kappa h}{2\beta}\left(K\Delta u^n_{s,0} - \frac{\sigma^n}{\rho_0-\sigma^n}\Delta u^n_{l,0}\right) = \mathcal{O}(h). \tag{58}$$

Thus, $\beta^n < \alpha^n$ for small enough values of h, and from $0 < 1 + z_j < 1$, one gets the positivity of $a^n_{s,j}$, while $c^n_{s,j} > 0$ unconditionally. In an analogous way, the positivity of coefficients $a^n_{l,j}$ and $c^n_{l,j}$ in the liquid phase scheme can be proved. Positivity of $b^n_{l,j}$ holds under the step sizes condition

$$k < \frac{h^2(\rho_0-\sigma^n)^2}{2}, \quad n_0 \le n \le n_1. \tag{59}$$

Note that (57) guarantees the inequality (59) when $\kappa < (\rho_0-\sigma^n)^2$. This means that the solidification front must satisfy $\sigma^n < \rho_0 - \sqrt{\kappa}$ and hence the integer n_1 defining the final time level of the second stage is

$$n_1 = \max\left\{n : \sigma^n < \rho_0 - \sqrt{\kappa}, \ ; n \ge n_0\right\}. \tag{60}$$

Note that the final of the second stage depends on the problem data and the initialization of the solid phase, i.e. of R_0.

Once the positivity of coefficients in (52) for $m = s, l$ has been shown under condition (57) for all time levels $n_0 \le n \le n_1$, where n_1 is given by (60), the stability of the temperatures sign comes from (53), obtaining the identity

$$a^n_{m,j} + b^n_{m,j} + c^n_{m,j} = 1, \quad m = s, l. \tag{61}$$

In fact, from (52)-(53), (61) and the positivity of coefficients $a^n_{m,j}$, $b^n_{m,j}$, $c^n_{m,j}$, assuming $-1 \le u^n_{s,j} \le 0$ and $0 \le u^n_{l,j} \le 1$, one gets not only the sign preserving but the boundedness property

$$\begin{cases} -1 \le u^{n+1}_{s,j} \le 0, & -M+1 \le j \le -1, \\ 0 \le u^{n+1}_{l,j} \le 1, & 1 \le j \le M. \end{cases} \tag{62}$$

The physics of the problem suggests that the temperatures in both phases increase with the spatial index j for each fixed time level n, $n_0 \le n \le n_1$. We show that the numerical solution preserves at this stage the monotonicity property under the stability and positivity conditions (57), (60) and small enough values of h.

From equations (52)-(53), positivity of coefficients $a^n_{s,j}$, $b^n_{s,j}$, $c^n_{s,j}$, and assuming that monotonicity property holds true up to time level n, it follows that,

$$u^{n+1}_{s,j+1} > (\alpha^n - (1+z_{j+1})\beta^n)u^n_{s,j} + (1-\alpha^n + (1+z_{j+1})\beta^n)u^n_{s,j+1}, \quad -M \le j \le -1, \tag{63}$$

and

$$u^{n+1}_{s,j} < (1-\alpha^n - (1+z_j)\beta^n)u^n_{s,j} + (\alpha^n + (1+z_j)\beta^n)u^n_{s,j+1}, \quad -M+1 \le j \le -1. \tag{64}$$

From (63) and (64) it follows that

$$u^{n+1}_{s,j+1} - u^{n+1}_{s,j} > (u^n_{s,j+1} - u^n_{s,j})(1 - 2\alpha^n + h\beta^n) > 0, \quad -M+1 \le j \le -1. \tag{65}$$

In analogous way, under previous conditions and small enough values of h, one gets

$$u^{n+1}_{l,j+1} > u^{n+1}_{l,j}, \quad 0 \le j \le M-1. \tag{66}$$

Summarizing, the following results have been established in this second stage:

Theorem 1. With previous notation, let n_0 be the positive integer chosen so that $\tau^{n_0} = \tau_0$ represents the end of the first stage, and let n_1 be defined by (60). Let $h > 0$ be the spatial stepsize and $k > 0$ the temporal stepsize, and let α^n and β^n defined by (53) for $n^0 \le n \le n^1$. If h and k satisfy (57) and $\beta^n < \alpha^n$ for $n^0 \le n \le n^1 - 1$, then the numerical scheme (52)-(53) and (55) preserves the sign, boundedness and the spatial monotonicity of both solid and liquid temperatures in the second stage, starting from the end of the first stage at time level n_0 and ending at time level n_1 given by the stability requirement (60).

Next example shows temperature profiles in both phases solid and liquid, at the end of the second stage.

Example 2 Figure 2 depicts numerical temperature distributions with respect to the variable z at the end of the second stage, i.e. $\tau_1 = 940.481$, both for the solid and the liquid phase. Model parameters take here the values $\kappa = K = \beta = 1$, step sizes $h = 0.05$, $k = 0.001$ and $R_0 = 0.03$. Note that in this instance, the position of the solidification front is given by the expression $\sigma(\tau_1) = \rho_0 - \sqrt{\kappa} = 32.3333$, i.e. the 97% of the material is solidified.

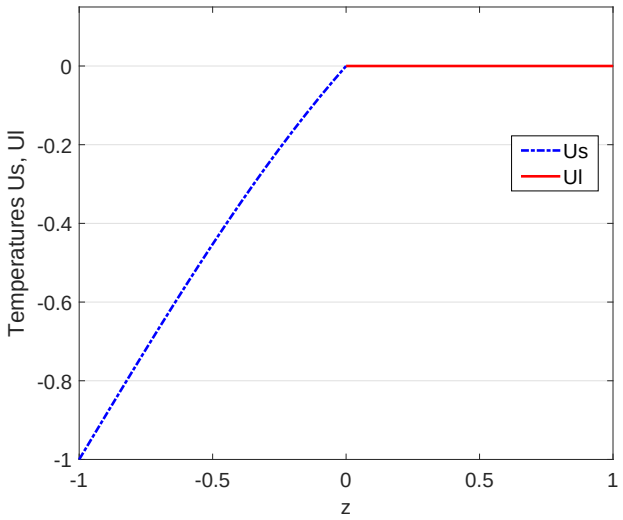

FIGURE 2 Numerical solutions for example 2 at the end of the second stage.

2.3 | Third stage numerical modelling

As it has been shown at the end of the second stage, the depletion of the liquid phase almost occurs and the temperature remains practically unaltered and close to zero. This fact completes numerically the idea suggested by the authors of[24], p. 270, about the time t^* when the liquid phase can be neglected.

Finally, for the third stage of the problem, within the time range $n_1 \leq n \leq n_2$, where n_2 corresponds to the time step such that $\sigma^{n_2} = \rho_0$, i.e. $\tau^{n_2} = \tau_e$ when the solid phase covers the entire domain. As in Section 2.2, the final conditions of the second stage are taken as initial conditions for the third one, while the boundary conditions continue unaltered, (37). In this third period, the formulation of the problem is changed by another, characterized only by the equation regarding the solid phase, (25), and the Stefan condition, that takes the form

$$\frac{d\sigma}{d\tau} = \frac{K}{\beta\sigma(\tau)} \frac{\partial U_s}{\partial z}, \quad z = 0, \quad \tau_1 < \tau < \tau_2. \tag{67}$$

The solution at the interior points at time level $n+1$, is given by the explicit scheme (52) for $m = s$, while the liquid phase is neglected. The properties of the numerical solution established in Theorem 1 remain preserved for the unique solid phase under that unique condition (57).

The discretization of the Stefan-like condition (67) takes the form

$$\frac{\sigma^{n+1} - \sigma^n}{k} = \frac{K}{\beta\sigma^n} \Delta u^n_{s,0}, \quad n_1 \leq n \leq n_2 - 1. \tag{68}$$

Note that comparing with the discretization of the change of the solidification front given by (55) in the second stage, here the second term of the right-hand side of (55) corresponding to the influence of the liquid phase into the solid-liquid interface is deleted.

In the following example, we illustrate the evolution of temperature profiles during all the stages, showing the properties of spatial monotonicity and stability, as well as the dynamics of the solidification front from the beginning until the extinction time.

Example 3 Figure 3 shows the results for the step sizes discretization $h = 0.002$ and $\Delta\tau = 0.01$ in the first stage, verifying conditions (43), and $h = 0.05$ and $k = 0.001$, under the hypothesis of Theorem 1. The solidified fraction at the end of the first stage is taken $R_0 = 0.03$ and the parameters of the model are $\kappa = K = \beta = 1$. Note that each curve corresponds to a different time; the first four upper curves correspond to increasing time values in the second stage, while the last one represents the temperature of the solid phase at the extinction time, i.e. the end of the third stage. The increasing behaviour of the temperatures is captured by the numerical solution and for the liquid phase the temperature is uniformly close to zero in the second stage. Figure 3 shows as the solidification front advances with the time and the slope of the temperature curve in the diminishing liquid phase approaches to zero due to the right end homogeneous Neumann boundary condition.

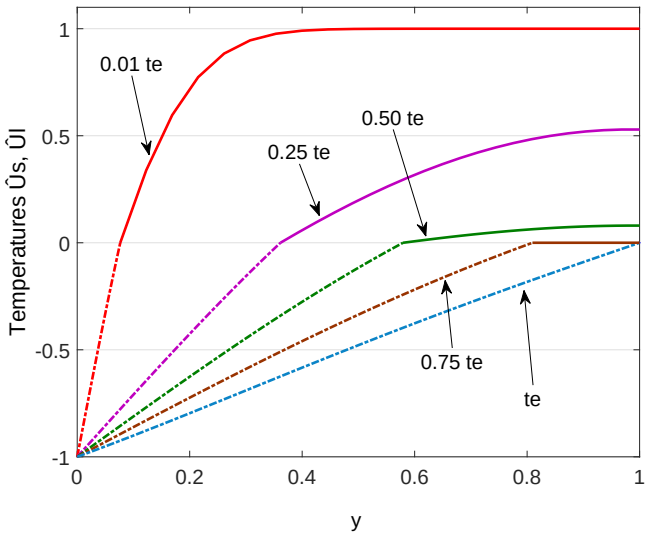

FIGURE 3 Numerical solutions for example 3 for different fractions of the extinction time. Dash-dot lines represent solid phase temperatures $\hat{U}_s$ and continuous lines show temperatures of the liquid phase $\hat{U}_l$.

Figure 4 shows the evolution of the solidification front. It agrees with the results of[24] using the Keller box scheme. The cooling impact in the advance speed of the solidification front is tempered by the effect of the liquid phase.

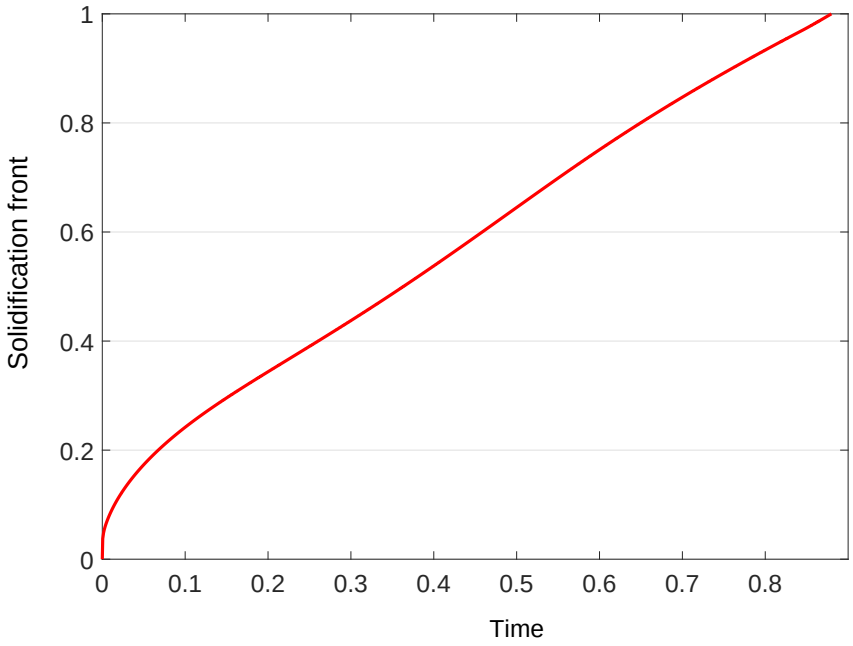

FIGURE 4 Numerical solidification front of example 3 as a function of time.

Table 2 contains a set of points covering the last quarter of the solidification process to study the change of behaviour of the original $C\sqrt{t}$-law due to the influence of the liquid phase.

Time t	0.6375	0.6800	0.7225	0.7650	0.8075	0.8500
Solidification front $\tilde{S}(t)$	0.7884	0.8288	0.8674	0.9043	0.9398	0.9741

TABLE 2 Solidification front $\tilde{S}(t)$ for large values of time.

These points $(t, \tilde{S}(t))$ have been matched to a curve of the form $\tilde{S}(t) = bt^{\alpha}$. A least square approach shows the optimal values $b = 1.09955$ and $\alpha = 0.73464$. The resulting coefficient of determination is $R^2 = 0.99963$.

The following Table 3 and Table 4 show, for different values of the temporal step size k, the relative error RE and the convergence rate γ, obtained for the numerical solutions of the solid and liquid temperatures $\hat{U}_s$ and $\hat{U}_l$ at points $y_s = 0.28082$ and $y_l = 0.78082$, located in the midpoint of each subdomain, at the instant $t = 0.42399$ when half of the 2^{nd} stage has elapsed.

$k_3 = 0.0005$	$k_1 = 0.001$	$k_2 = 0.00075$
RE	1.47402e-06	7.03169e-07
γ	-	1.82545

TABLE 3 Relative error RE and convergence rate γ for the solid temperature solutions, taking $k_3 = 0.0005$ as the reference step size and $h = 0.05$ in all cases.

$k_3 = 0.0005$	$k_1 = 0.001$	$k_2 = 0.00075$
RE	9.69036e-05	4.56845e-05
γ	-	1.85456

TABLE 4 Relative error RE and convergence rate γ for the liquid temperature solutions, taking $k_3 = 0.0005$ as the reference step size and $h = 0.05$ in all cases.

Although the first and third stages are qualitative relevant due to the issues of initialization and depletion, it is important to point out that both from the spatial and temporal points of view both stages have a reduced quantitative significance versus the second stage. This facts are illustrated in Figure 5 , where $R_0 = 0.03$, $t_e = 0.881195$ and $\tau_e = 979.106$ for the data in this example.

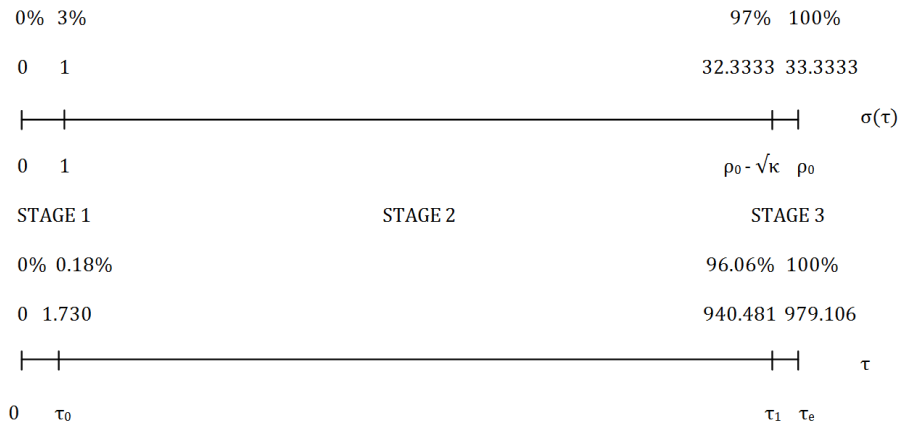

FIGURE 5 Above: Spatial stages distribution. Below: Time stages distribution.

Next example illustrates the fact that both the extinction time and temperatures in the solid phase for complete depletion does not change significantly for changes in a small enough R_0.

Example 4 Let us take three chosen values of the fraction R_0. For the model parameters $\kappa = K = \beta = 1$ and taking $h = 0.002$, $\Delta\tau = 0.01$ in the first stage, $h = 0.05$, $k = 0.001$ in the second and third stage, Table 5 shows the times t_0 when finishes the first stage, t_1 at the end of the second stage and t_e, as well as the root mean squared error (RMSE) of the distribution of the temperature of the solid at t_e with respect to the lower value of $R_0 = 0.01$.

R_0	t_0	t_1	t_e	% 2nd stage	RMSE	CPU time (seconds)
0.05	0.004750	0.820648	0.876230	93.11	0.0228	79.79
0.03	0.001557	0.846433	0.881195	95.88	0.0127	205.09
0.01	0.000103	0.873104	0.885353	98.60	——	2067.11

TABLE 5 Dependence of t_0, t_1, t_e and RMSE of temperatures on the fraction R_0, when the parameters of the model are $\kappa = K = \beta = 1$.

CONCLUSION

In this paper two-phase solidification Stefan problems in a finite domain are treated numerically, including the formation and depletion stages. Numerical solutions obtained with the proposed schemes become stable and preserve the qualitative properties of the theoretical solutions. In particular, the spatial monotonicity of the temperatures at all temporal levels is shown.
The treatment does not require the knowledge of the analytical solution of the problem into a semi-infinite medium, allowing the possibility of potential application to more complex problems such as cryosurgery, where cancer cells may be destroyed under extremely cold temperatures.

ACKNOWLEDGMENTS

This work has been partially supported by the Ministerio de Ciencia, Innovación y Universidades, Spanish grant MTM2017-89664-P.
There are no conflicts of interest to this work.

References

1. Crank J.. *Free and moving boundary problems*. Oxford University Press; 1984.

2. Gupta S.C.. *The classical Stefan problem, Volume 45, 1st Edition. Basic concepts, modelling and analysis*. JAI Press; 2003.

3. Schmidt A.. Computation of three dimensional dendrites with finite elements. *Journal of Computational Physics.* 1996;125(2):293–312.

4. Singh S., Bhargava R.. Simulation of phase transition during cryosurgical treatment of a tumor tissue loaded with nanoparticles using meshfree approach. *Journal of Heat Transfer.* 2014;136(12):121101–10.

5. Company R., Egorova V., Jódar L.. Solving American option pricing models by the front fixing method: numerical analysis and computing. *Abstract and Applied Analysis.* 2014;2014:ID 146745–9.

6. Griewank P. J., Notz D.. Insights into brine dynamics and sea ice desalination from a 1 - D model study of gravity drainage. *Journal of Geophysical Research: Oceans.* 2013;118(7):3370–3386.

7. Javierre E., Vuik C., Vermolen F.J., Zwaag S.. A comparison of numerical models for one-dimensional Stefan problems. *Journal of Computational and Applied Mathematics.* 2006;192:445–459.

8. Briozzo A.C., Natale M.F., Tarzia D.A.. Explicit solutions for a two-phase unidimensional Lamé-Clapeyron-Stefan problem with source terms in both phases. *Journal of Mathematical Analysis and Applications.* 2007;329(1):145–162.

9. Caldwell James, Chan Ching-Chuen. Spherical solidification by the enthalpy method and the heat balance integral method. *Applied Mathematical Modelling.* 2000;24(1):45–53.

10. Chantasiriwan S., Johansson B.T., Lesnic D.. The method of fundamental solutions for free surface Stefan problems. *Engineering Analysis with Boundary Elements.* 2009;33(4):529–538.

11. Hon Y. C., Li M.. A computational method for inverse free boundary determination problem. *International Journal for Numerical Methods in Engineering.* 2008;73(9):1291–1309.

12. Rizwan-Uddin . A nodal method for phase change moving boundary problems. *International Journal of Computational Fluid Dynamics.* 1999;11(3–4):211–221.

13. Caldwell J., Kwan Y.Y.. On the perturbation method for the Stefan problem with time-dependent boundary conditions. *International Journal of Heat and Mass Transfer.* 2003;46(8):1497–1501.

14. Stephan K., Holzknecht B.. Perturbation solutions for solidification problems. *International Journal of Heat and Mass Transfer.* 2017;(19):597–602.

15. Savović S., Caldwell J.. Finite difference solution of one-dimensional Stefan problem with periodic boundary conditions. *International Journal of Heat and Mass Transfer.* 2003;46(15):2911–2916.

16. Kutluay S., Bahadir A.R., Özdeş A.. The numerical solution of one-phase classical Stefan problem. *Journal of Computational and Applied Mathematics.* 1997;81(1):135–144.

17. Asaithambi N.S.. A variable time step Galerkin method for a one-dimensional Stefan problem. *Applied Mathematics and Computation.* 1997;81(2):189–200.

18. Goodman T.. The heat-balance integral and its application to problems involving a change of phase. *Trans. ASME.* 1958;80(2):335–342.

19. Landau H.G.. Heat conduction in a melting solid. *Quarterly Applied Mathematics.* 1950;8:81–95.

20. Churchill S.W., Gupta J.P.. Approximations for conduction with freezing or melting. *International Journal of Heat and Mass Transfer.* 1977;20(11):1251–1253.

21. Kutluay S., Esen A.. An isotherm migration formulation for one-phase Stefan problem with a time dependent Neumann condition. *Applied Mathematics and Computation.* 2004;150(1):59–67.

22. Esen A., Kutluay S.. A numerical solution of the Stefan problem with a Neumann-type boundary condition by enthalpy method. *Applied Mathematics and Computation.* 2004;148(2):321–329.

23. Voller V.R., Cross M.. Applications of control volume enthalpy methods in the solution of Stefan problems. In: Lewis R.W., Morgan K., Johnson J.A., Smith W.R., eds. *Computational Techniques in Heat Transfer*, Pineridge Press Ltd., Mambles, Swansea, UK 1985.

24. Mitchell S.L., Vynnycky M.. On the accurate numerical solution of a two-phase Stefan problem with phase formation and depletion. *J. Comput. Appl. Math.*. 2016;300(C):259–274.

25. Meek P.C., Norbury J.. Nonlinear moving boundary problems and a Keller Box scheme. *SIAM Journal on Numerical Analysis.* 1984;21(5):883–893.

26. Tarzia D.A.. Relationship between Neumann solutions for two-phase Lamé-Clapeyron-Stefan problems with convective and temperature boundary conditions. *Thermal Science.* 2017;21(1A):187–197.

27. Smith G.D.. *Numerical solution of partial differential equations: finite difference methods*. Oxford: Clarendon Press; 3rd ed.1985.

28. Plemmons R.J.. M-matrix characterizations. I-Nonsingular M-matrices. *Linear Algebra and its Applications.* 1977;18(2):175–188.

29. Axelsson O.. *Iterative Solution Methods*. Cambridge University Press, NY, USA; 1994.